Supporting Information

Semi-Quantitative Design of Black Phosphorous Field-Effect Transistor Sensors for Heavy Metal Ion Detection in Aqueous Media

Jingbo Chang[1†], Haihui Pu[1†], Spencer A. Wells[2], Keying Shi[4], Xiaoru Guo[1], Guihua Zhou[1], Xiaoyu Sui[1], Ren Ren[1], Shun Mao[1,5], Yantao Chen[1], Mark C. Hersam[2,3], Junhong Chen[1]*

[1]Department of Mechanical Engineering, University of Wisconsin-Milwaukee, 3200 North Cramer Street, Milwaukee, Wisconsin, 53211, USA

[2]Department of Materials Science and Engineering, Northwestern University, Evanston, Illinois, 60208, USA

[3]Department of Chemistry, Northwestern University, Evanston, Illinois, 60208, USA

[4]Key Laboratory of Functional Inorganic Material Chemistry, Ministry of Education of the People's Republic of China, Heilongjiang University, Harbin 150080, P. R. China

[5]State Key Laboratory of Pollution Control and Resource Reuse, School of Environmental Science and Engineering, Tongji University, 1239 Siping Road, Shanghai 200092, P.R. China

[†]These authors contributed equally to this work.

Correspondence and requests for materials should be addressed to J.H.C. (email: jhchen@uwm.edu).

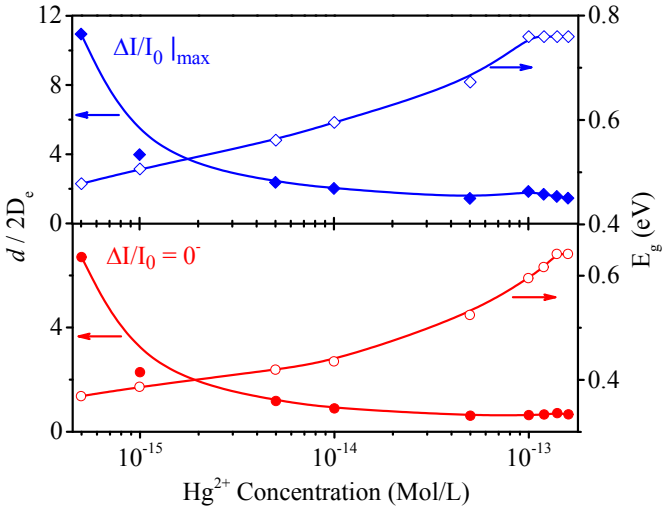

Figure S1. Relationship between $d/2D_e$ and Hg^{2+} concentrations. The ratio $d/2D_e$ (left axis) and the band gap E_g in BP (right axis) corresponding with $\Delta I/I_0|_{max}$ and $\Delta I/I_0=0^-$ with respect to the Hg^{2+} concentration.

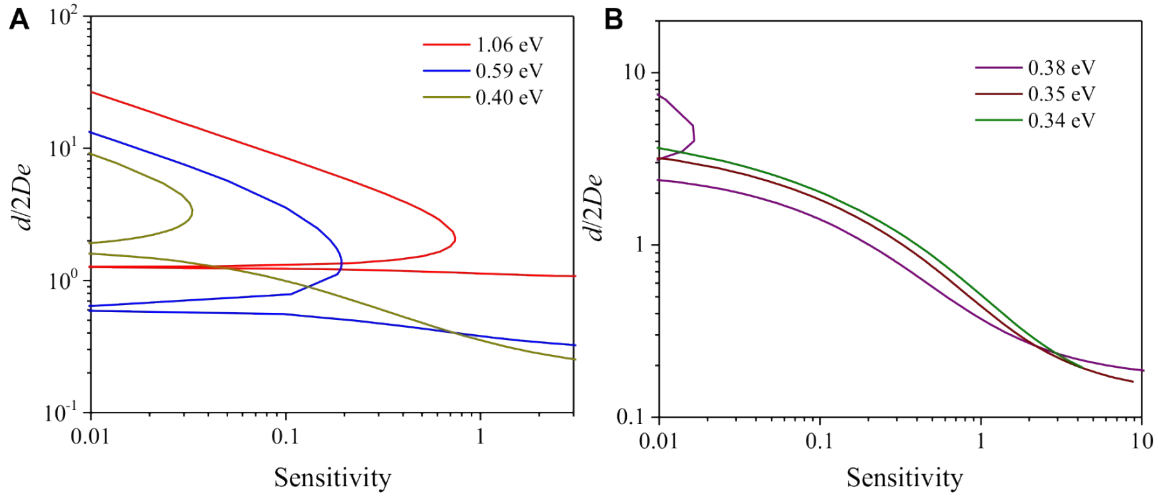

Figure S2. The ratio $d/2D_e$ with respect to the sensitivity: for band gap $E_g \geq 0.40$ eV and $E_g < 0.40$ eV in (A) and (B), respectively.

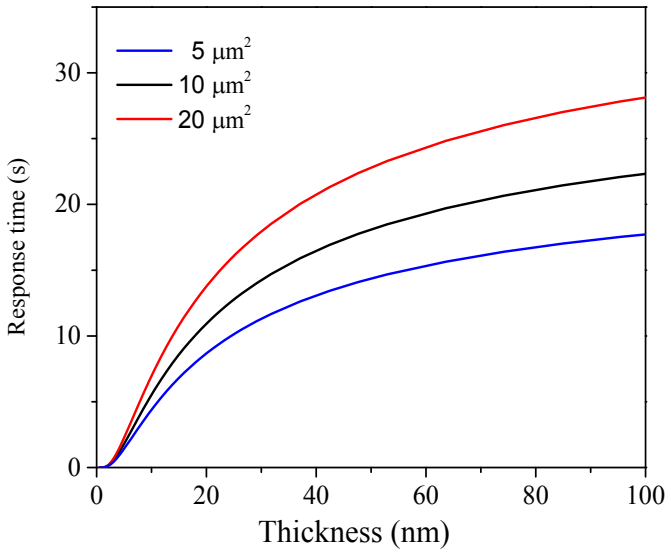

Figure S3. The predicted dynamic response time of BP with respect to its thickness for different BP surface areas.

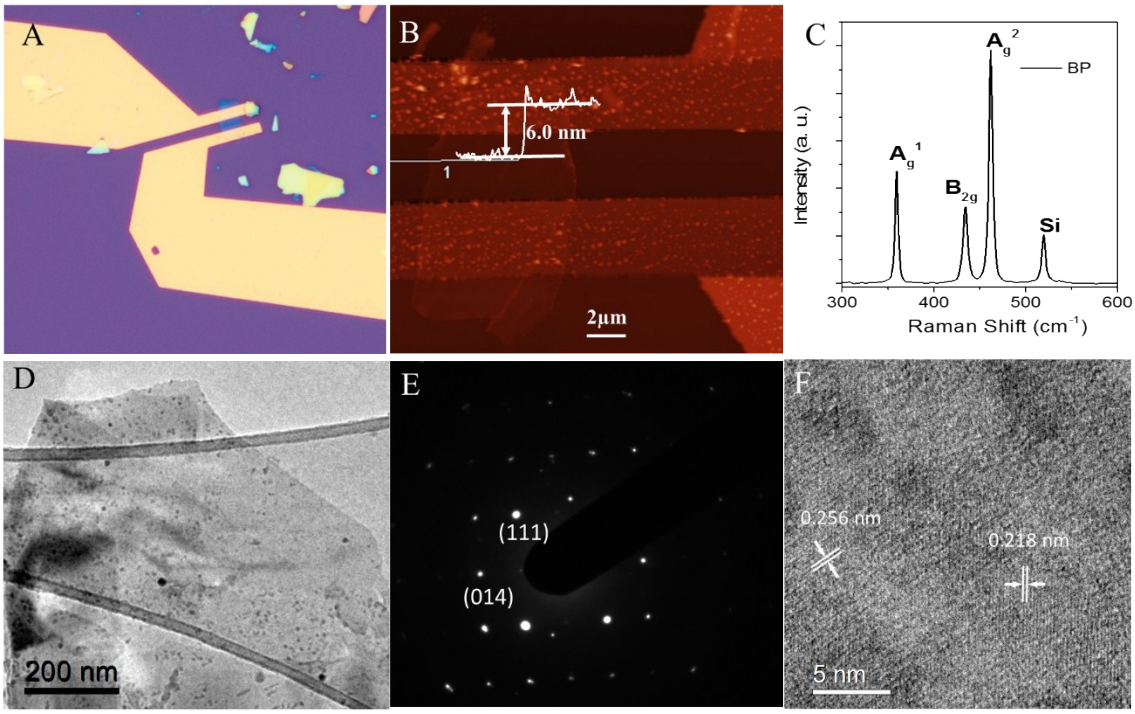

Figure S4. Multilayer BP-based FET sensor and its structural characterization. (A) The optical image of the BP flake across the electrodes. (B) An AFM image of the BP flake in (A) with the height profile indicating the thickness of the multilayer BP (~6.0 nm). (C) Raman spectrum of multilayer BP. (D-F) The TEM image, the SAED pattern, and the HRTEM image of BP, respectively.

To characterize the structural properties of as-made BP, Raman spectrum from 300 to 600 cm^{-1} was monitored. We can see from Fig. S4 C that four distinct peaks are clearly observed at 362.1 cm^{-1}, 439.5 cm^{-1}, 467.7 cm^{-1} and 520.9 cm^{-1}, with the former three and the last one associated with BP and Si, respectively. The peaks centered at 362.5 cm^{-1}, 439.8 cm^{-1} and 467.1 cm^{-1} are attributed to the A^1_g, B_{2g} and A^2_g phonon modes observed in bulk BP. Figure S4 D shows the transmission electron microscopy (TEM) image of an exfoliated BP flake transferred onto the holey carbon grid. The selected area electron diffraction (SAED) pattern in Fig.S4 E indicates a single crystalline structure. Figure S4 F presents the high-resolution TEM (HRTEM) image with lattice spacings of 0.256 and 0.218 nm, corresponding with the (111) and (020) planes of side-centered orthorhombic BP, respectively. The Raman spectrum in Fig. S4 C and the TEM characterizations in Fig. S4 D-F reveal the high crystalline quality of the as-made BP flake in our FET sensors.

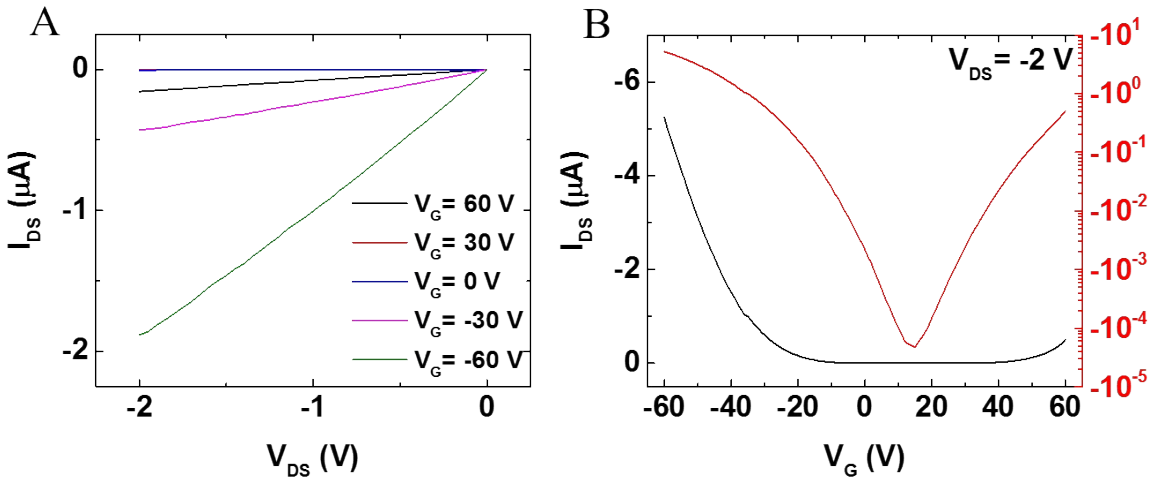

Figure S5. The output and transfer characterization of BP sensor. (A) The output and (B) the transfer characteristics of the 6.0 nm-thick BP flake. The transfer curve in (B) is in the linear (left axis) and logarithmic (right axis) scales, respectively. Note that the IV curves in (A) for the gate voltages at 0 V and 30 V nearly overlap with each other in the linear scale plot, and thus it is hard to distinguish visually. The linear output curve in (A) implies an Ohmic-like contact between the Au electrodes and BP, suggesting an effective carrier injection from the Ni electrodes into BP, as well as the minimization of the potential electrical noise from the mechanical perturbation during the sensing test. The transfer characteristics of our BP FET device in (B) exhibits a well-developed saturation curve of p-type nature with an on/off current ratio up to 10^5.

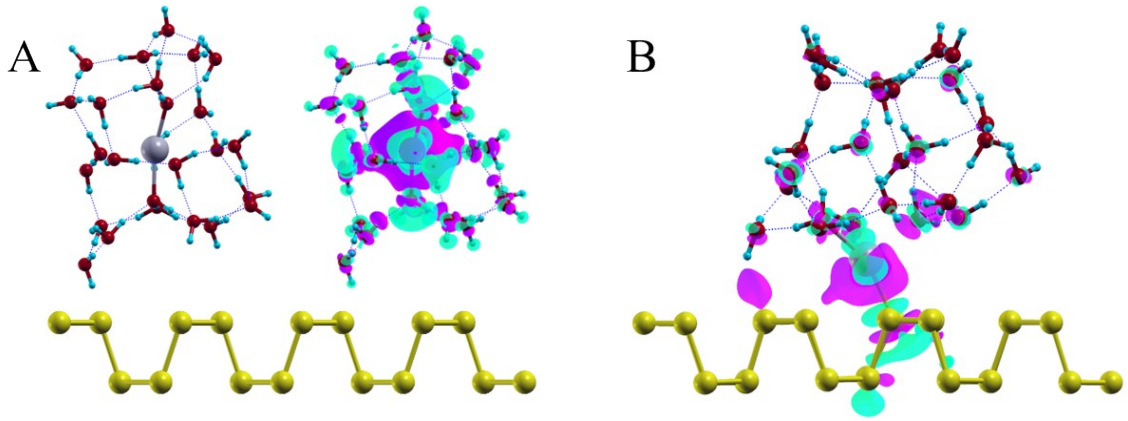

Figure S6. Adsorption of Hg^{2+} ions on BP. (A) Upper left: structure of a mercury ion (Hg^{2+}) embedded in a small water droplet; upper right: the difference charge density distribution of Hg^{2+} inside the water droplet; lower panel: side view of the monolayer BP. (B) The difference in charge density distribution of Hg^{2+} upon adsorption on the surface of monolayer BP. In both (A) and (B), the yellow, red, cyan, and gray balls represent the phosphorus, oxygen, hydrogen atoms, and mercury ions, respectively. The isosurface value in the difference charge density is 2.5×10^{-3} e/Bohr^3, while the purple- and cyan-coded regions indicate the electron accumulation and depletion, respectively. The blue dotted lines represent the hydrogen bonds.

The probe-free detection of Hg^{2+} ions with high sensitivity can be partly ascribed to the unique structure of BP. This is because only three tetrahedral-like bonds are formed that are associated with the orbital hybridization (sp^3-like) but out of five valence electrons, thus leaving two effective orbitals dangling, which also can be seen from the charge density of states that the top valence and bottom conduction band are primarily occupied by the *P*z orbitals.[1] Consequently, the lone electrons of phosphorus atoms give rise to the probe-free detection of metal ions. Nevertheless, the contribution of Hg^{2+} ions is even more important. As the positively charged metal ions oxidize, they attract electrons from BP. In our experiments, since the metal ions were diluted in the DI water, we started the simulations with the metal ions in the water environment, as illustrated in Figure S6A, in which Hg^{2+} is embedded in a water droplet. The oxidizing nature of the positively charged Hg^{2+} enables it to attract charge from the water environment, as evidenced by the difference in charge density in Figure S6A, in which the charge is transferred from the water molecules and accumulated in Hg^{2+}. Upon adsorption on the BP surface, Figure S6B indicates that Hg^{2+} forms a bond with the underlying phosphorus atom and gains electrons.

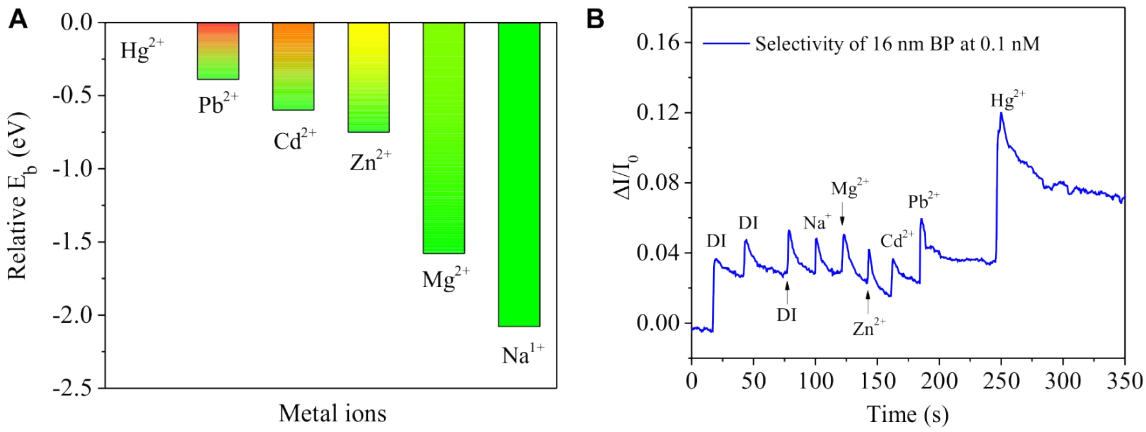

Figure S7. Selectivity of BP sensor. (A) The relative binding energies E_b of metal ions with respect to that of mercury ions. E_b is defined as $E_b = E_{BP} + E_{metal\ ion} - E_{BP+metal\ ion}$, where E_{BP}, $E_{metal\ ion}$, and $E_{BP+metal\ ion}$ are the total energies of isolated BP, isolated metal ions, and BP with metal ions adsorbed on its surface, respectively. (B) Dynamic responses of the BP FET sensor to various metal ions (Na^+, Mg^{2+}, Zn^{2+}, Cd^{2+}, Pb^{2+}, Hg^{2+}) at 0.1 nM.

For the same BP sensor device, the adsorption strength of various metal ions are governed only by their capability in gaining charges. In fact, the ability of an atom to gain or lose electrons can be described by its electronegativity: the higher the electronegativity of an atom, the greater its ability to withdraw electrons. This trend also holds for the metals ions with same valence charges, especially for the elements in (near) the same row/column. For example, the elements in terms of electronegativity (the number in the parenthesis) can be arranged in the order of Hg (1.9) > Pb (1.8) > Cd (1.7) > Zn (1.6) > Mg (1.2) > Na (0.9) from the Pauling scale,[2,3] suggesting the relative sensitivity in such an order for any sensing materials, in excellent agreement with the predicted interaction strength trend in Figure S7A. To further confirm this sensitivity trend, a 16 nm-thick BP sensor was tested for these metal ions in DI water. Figure S7B presents the dynamic response in terms of $\Delta I/I_0$ with respect to these metal ions at a concentration of 0.1 nM. The amplitude of current increase suggests that the sensor is specific to Hg^{2+} at 0.1 nM, with the sensitivity/relative current change (0.05) being five times of that (0.01) towards Pb^{2+}, while Na^+, Mg^{2+}, Zn^{2+}, and Cd^{2+} ions lead to negligible current increases upon adsorption. Consequently, the moderate oxidizing ability of Hg^{2+} gives rise to its sensitive, selective, and probe-free detection, which also could be realized by other semiconducting sensor materials if the band gap of the sensor material is in a suitable range.

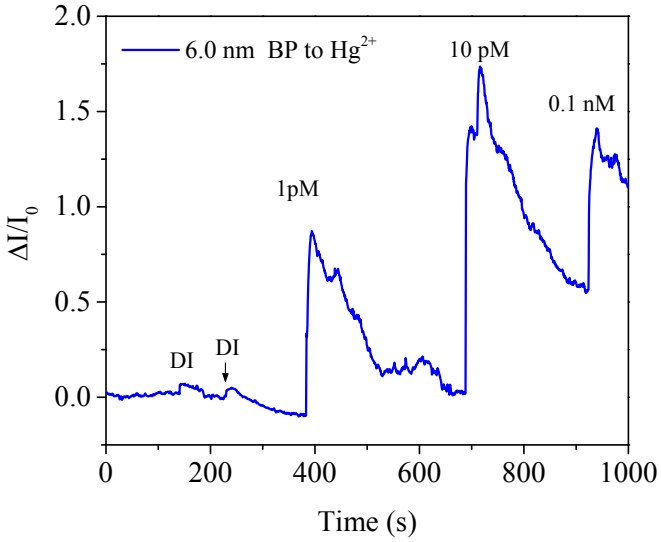

Figure S8. Dynamic response to Hg^{2+} ion with varying concentrations at a BP thickness of 6.0 nm. The baseline continues decreasing throughout the measurements due to ongoing oxidation. Moreover, the current decreases even upon Hg^{2+} ion adsorption, primarily because thin BP is more easily oxidized, thereby increasing the resistance of BP.

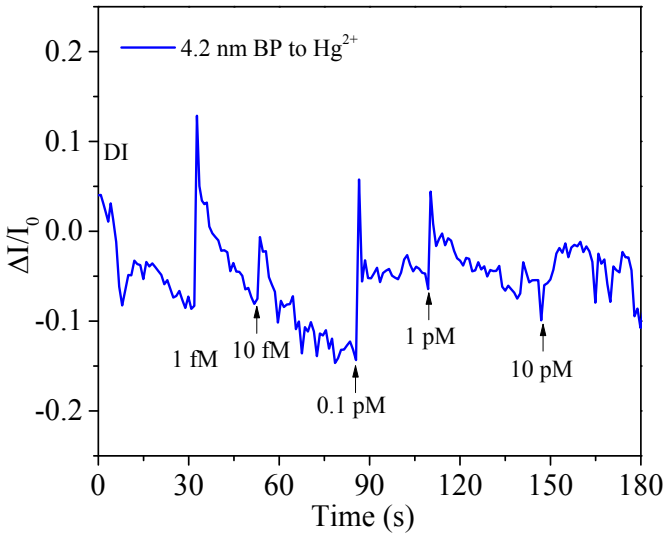

Figure S9. Dynamic response to Hg^{2+} ion with varying concentrations at a BP thickness of 4.2 nm. The noisy signal results from the fact that thin BP is very unstable, which is expected. The sensor barely responded to Hg^{2+} at various concentrations (from 1 fM to 10 pM), except that the current dropped below the initial value.

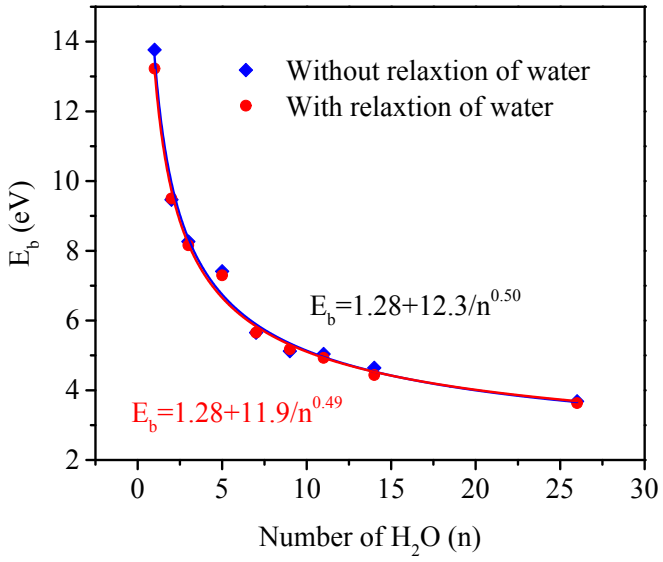

Figure S10. The binding energy E_b of Hg^{2+} with respect to the number n of water molecules on phosphorene. The solid curves are the nonlinear fittings. E_b (Hg^{2+}) is calculated as the difference between the binding energies of the water droplet with and without Hg^{2+}, namely, $E_b(Hg^{2+}) = E_b(Hg^{2+}+nH_2O) - E_b(nH_2O)$. Here, two scenarios are considered for the calculation of E_b (nH_2O). We started with the optimized structure of Hg^{2+} adsorbed on the surface of phospherene with the water droplets surrounding the Hg^{2+}, as demonstrated in Figure S6B, then Hg^{2+} was removed and the system energy was calculated with and without the relaxation of water droplets, respectively. Despite the small difference between E_b (Hg^{2+}) with a small number of water molecules, this difference should be zero with the infinitely large number of water molecules. Therefore, the final E_b (Hg^{2+}) should be the same during the fitting procedure.

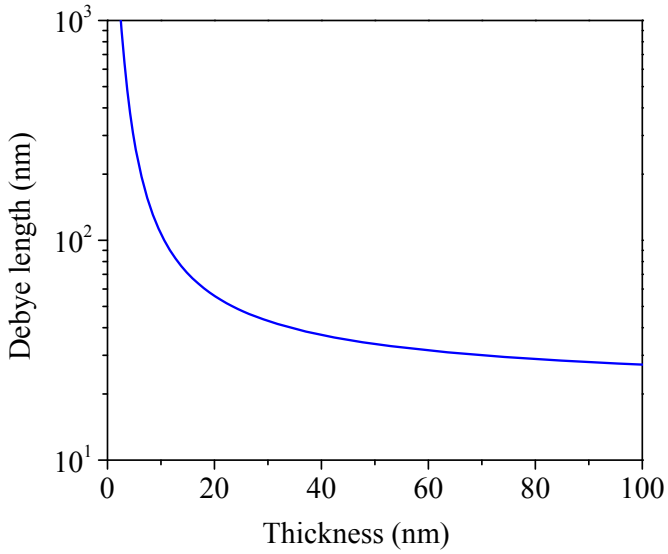

Figure S11. The Debye screening length of BP as a function of BP thickness.

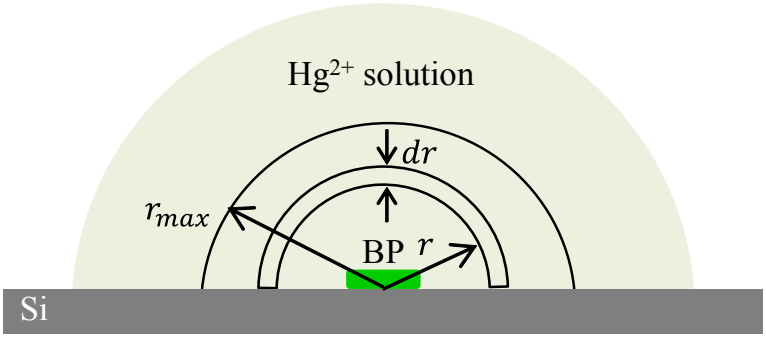

Figure S12. Schematic of the region in the droplet of Hg^{2+} solution within which the Hg^{2+} ions diffuse and adsorb on the surface of BP. Here, r_{max} indicates the maximum radius of the semisphere beyond which Hg^{2+} ions cannot be adsorbed.

Supplementary Methods

Metal ion adsorption density

For the metal ion solution, the Gibbs free energy G of the system is[4]

$$G = k_B T \sum_i N_i \left(ln\lambda_i^3 \rho_i + ln\gamma_i \right) + F_{el}, \quad \lambda_i = h/\sqrt{2\pi m_i k_B T} \tag{S1}$$

where k_B is the Boltzmann constant, T is constant, h is Planck's constant, N_i is the number of metal ion of species *i*, ρ_i is the metal ion concentration (i.e., the number density), m_i is the mass of metal ion, γ_i is the activity coefficient, and F_{el} is the electrostatic energy. At the Debye-Hückel limit, the activity and electrostatic energies are

$$k_B T \sum_i N_i ln\gamma_i = -\frac{\sum_i N_i z_i^2 e^2}{2\varepsilon(\lambda_D + a)} + \frac{4\pi}{3} k_B T \sum_i N_i \rho_i a_i^3, \quad \lambda_D = \left(\frac{4\pi e^2}{\varepsilon k_B T} \sum_i \rho_i z_i^2\right)^{-\frac{1}{2}}$$

(S2)

$$F_{el} = -\frac{e^2}{2\varepsilon k_B T \lambda_D} \sum_i N_i z_i^2 = -\frac{V}{8\pi\lambda_D^3} \tag{S3}$$

where ε is the permittivity of the metal ion solution, z_i is the charge of the metal ion *i*, *e* is the elementary charge, a_i is the diameter of the metal ion *i*, *V* is the volume of the system. At high dilutions, $\lim_{\rho_i \to 0} ln\gamma_i = 0$, then

$$G = k_B T \sum_i N_i ln\lambda_i^3 \rho_i - \frac{V}{8\pi\lambda_D^3} \quad \text{(S4)}$$

From the thermodynamics relationship, $dG = VdP - SdT$, in which *P* is the osmotic pressure in the solution and *S* is the entropy, we have

$$V(\frac{\partial P}{\partial V})_{N,T} = (\frac{\partial G}{\partial V})_{N,T} \quad \text{(S5)}$$

Plugging $\rho_i = N_i/V$ into Equation (S4) and λ_D and then take the derivative with respect to *V*, we obtain

$$(\frac{\partial G}{\partial V})_{N,T} = -\frac{1}{V} k_B T \sum_i N_i - \frac{V^{-\frac{3}{2}}}{16\pi} (\frac{4\pi e^2}{\varepsilon k_B T} \sum_i \rho_i z_i^2)^{\frac{3}{2}} \quad \text{(S6)}$$

Multiply both sides of Equation (S5) by dV/V and then insert Equation (S6) and integrate from V to ∞,

$$\int_V^\infty \frac{\partial P}{\partial V} dV = -k_B T \sum_i N_i \int_V^\infty \frac{1}{V} dV - \frac{1}{16\pi} (\frac{4\pi e^2}{\varepsilon k_B T} \sum_i \rho_i z_i^2)^{\frac{3}{2}} \int_V^\infty V^{-\frac{5}{2}} dV \quad \text{(S7)}$$

After some algebra, we obtain

$$\frac{p}{k_B T} = \sum_i \rho_i - \frac{1}{24\pi\lambda_D^3} = \sum_i \rho_i (1 - \frac{z_i^2 l_B}{6\,\lambda_D}) \quad \text{(S8)}$$

Namely,

$$\frac{p_i}{k_B T} = \rho_i (1 - \frac{z_i^2 l_B}{6\,\lambda_D}), \quad \text{(S9)}$$

which shows that the partial osmotic pressure p_i of metal ions *i* is simply related to its concentration ρ_i, the Bjerrum length l_B, the Debye length λ_D of the metal ion solution, and the number of valence charge z_i of metal ion *i*.

We now turn to the underlying physics behind the Debye-Hückel approximation. For electrolyte with a low concentration, the distance between the ions is so large that the interactions among the ions could be neglected. This is reasonable since λ_D=30.4 nm is greatly larger than the Bjerrum length l_B (0.71 nm) at room temperature for an aqueous 1-1 electrolyte solution at a concentration of 100 μM/L. For our sensor testing, the concentration of metal ions are several orders of magnitude below 1 μM/L. At such low concentrations, the Debye-Hückel approximation is even more accurate. Consequently, the partial osmotic pressure p_i of metal ions *i* can be reduced only related to its number density ρ_i. Moreover, the electrolyte could be in effect treated as an "ideal gas" mixture of ions in a continuum dielectric medium (DI water here) of dielectric constant, and the ideal gas model can be adopted here. We have previously shown that the adsorption density for ideal gas is[5]

$$n_a = \frac{p_g \lambda^3}{k_B T} \prod_{i=x,y,z} q_i exp(-\frac{\Delta E_G}{k_B T}), \quad \text{(S10)}$$

where p_g is the partial pressure of the target gas, q_i is the directional partition function, ΔE_G is the Gibbs free energy change after the gas adsorption and is negative for adsorption. With Equation (S9), the adsorption density of metal ions is thus

$$n_a = \rho_i \lambda^3 \prod_{i=x,y,z} q_i exp(-\frac{\Delta E_G}{k_B T}). \quad \text{(S11)}$$

The partition function along the vertical direction is $q_z = \sum_{n=1} exp(-E_n/k_B T)$, where E_n is the adsorption energy level. The precise value of E_n can only be obtained by fitting the interaction

potential between the ions and the underlying materials first and then solving the Schrödinger Equation. This procedure is quite cumbersome. Practically, q_z can be approximated by $exp(-E_0/k_BT) = exp(-\Delta E_G/k_BT)$ with only slight underestimate. Thus, Equation (S11) could be reformulated as

$$n_a = \rho_i \lambda^3 \prod_{i=x,y} q_i exp(-\frac{2\Delta E_G}{k_B T}) \quad \text{(S12)}$$

For the metal ion adsorption, especially for those strongly oxidizing ions (e.g., Hg^{2+}), the interaction strength between the metal ion and the underlying material is so strong that the surface adsorbed metal ions are localized and can be treated as the harmonic oscillators. In this case, the in-plane partition function is approximated as $q_i = \sum_{n=0}^{\infty} exp(-nhv/k_BT)$, where υ is the frequency of the oscillator and is typically in the order of THz at 300K.

The Gibbs free energy change is

$$\Delta E_G = \left(E_{ion+H_2O} - E_{ion} - E_{H_2O}\right) + E_{ZP} - T(0 - S) = -E_b + E_{ZP} + TS, \quad \text{(S13)}$$

where E_{ion+H_2O} is the system energy after the ion adsorption, E_{ion} is the energy of ion, and E_{H_2O} is the energy of the aqueous solution. The energy difference before and after the ion adsorption is the adsorption energy of metal ion (negative of the binding energy E_b). E_{ZP} is the zero point energy of the adsorbed ions and is on the order of k_BT. S is the entropy of the ions, and is 0.35 eV for Hg^{2+}.[6,7] Here the binding energy E_b can be obtained from the first-principles calculations. Given that the ions in the solution are surrounded by an infinitely large number of water molecules, this is not possible for realistic calculations. However, this obstacle can be circumvented via the extrapolation method. Technically, we can calculate E_b with respect to the number of water molecules and then extrapolate it at the infinite limit of water molecules by fitting the relationship between E_b and the number of water molecules. Figure S10 shows the binding energy E_b as a

function of number of water molecules for monolayer BP (i.e., phosphorene). After the fitting, we are able to extrapolate E_b of 1.28 eV for Hg^{2+} adsorption. Since the band gap of BP is thickness dependent, and this is also the case for E_b. Here, we use our previous extrapolation method for gas adsorption[1] to extract the layer dependent E_b for Hg^{2+} adsorption on BP. With these results, the Hg^{2+} adsorption density can be obtained using Equation (S12) as a function of thickness of BP.

Metal ion adsorption induced conductance change

The sensitivity S of the FET sensor is defined as the conductance change after the metal ions adsorption normalized to its initial value, namely,

$$S = \frac{\Delta\sigma}{\sigma_0} = \frac{\sigma - \sigma_0}{\sigma_0} = \frac{I/V - I_0/V}{I_0/V} = \frac{enu - en_0u_0}{en_0u_0} = \frac{nu - n_0u_0}{n_0u_0}, \quad \text{(S14)}$$

in which $(\sigma_0)\ \sigma$, $(n_0)\ n$, $(u_0)\ u$ are the (initial) conductance, carrier concentration, carrier mobility, respectively, and e is the elementary charge. Since during the sensing tests, the source drain voltage is fixed, the sensitivity can also be defined in terms of current I instead of conductance. Because hole is the major carrier in the p-type BP, Equation (S13) can be more clearly expressed as

$$S = \frac{n_hu - n_{h0}u_0}{n_{h0}u_0}, \quad \text{(S15)}$$

where n_{h0} and n_h are the hole concentration before and after the metal ions adsorption. In p-type semiconductors, the hole concentration is

$$n_{h0} = 2\left(\frac{2\pi m_h^* k_B T}{h^2}\right)^{\frac{3}{2}} exp\left(-\frac{E_g}{2k_BT}\right) exp\left(-\frac{E_F - E_{Fi}}{k_BT}\right), \quad \text{(S16)}$$

in which m_h^* is the effective mass of hole, E_g is the band gap, $(E_{Fi})E_F$ is the (intrinsic) Fermi level. All these values can be obtained from the reported results.[8-10]

After the metal ions adsorption, the charge transfer occurs, irrespective of the metal ion adsorption density, and thus leads to the carrier concentration redistribution. The carrier can only

be uniformly redistributed when the thickness of BP is on the order of Debye screening length at room temperature. Figure S11 shows the predicted Debye length of BP. We can see that D_e decreases as the thickness of BP increases. At 100 nm, D_e is 27 nm. For 100 nm-thick BP, the metal ions adsorption induced carrier concentration change decays from the top region into and bottom one. The decay coefficient at the bottom region is $\exp\left(-\delta/D_e\right)$=0.02. Despite small, we can still make the approximation that the charge penetrates into the entire BP, and this penetration is more thorough upon the application of external source drain voltage. Consequently, we assume that the metal ion adsorption induced carrier concentration is uniformly distributed through the entire BP flake when its thickness is less than 100 nm.

Upon the metal ion adsorption, its instant effect is three-fold. First, each metal ion gains Δq_a^+ electron from the underlying material, while the total amount of transferred charge per unit area is $n_a \Delta q_a^+$. Second, the surface adsorbed metal ions are still individually positively charged by Δq_g^-. They act as the scattering centers to the hole carrier in the underlying material and lead to the degradation of hole mobility. The degree of this degradation depends on both the distance d between the adsorbed metal ions and the Debye length D_e in the underlying material. Empirically, the hole mobility u degrades in the exponential form as

$$\mu = \mu_0[1 - \exp\left(-\alpha\frac{d}{D_e}\right)], D_e = \sqrt{\frac{\varepsilon\varepsilon_0 k_B T}{e^2 n_{h0}}}, \quad \text{(S17)}$$

where α is parameter, ε is the relative permittivity of the underlying material. Third, the density of metal ion adsorption is high, and the positivity charged metal ions further collectively form an effective gate voltage, which pushes the hole carrier away and results in the decrease of hole concentration. Moreover, the hole concentration decrease is positively related to its mobility degradation. The more severely the hole carrier mobility is degraded, the larger the hole concentration is reduced. As each metal ion can maximally repels Δq_g^- holes, the number of

repelled holes depends on the hole mobility in the form of $(1 - u/u_0)$. Consequently, the carrier concentration change upon the metal ion adsorption can be finally formulated as

$$n_h = [n_a \Delta q_a^+ - n_a \Delta q_g^- exp\left(-\alpha \frac{d}{D_e}\right)]/\delta + n_{h0} \quad \text{(S18)}$$

With Equation (S12), (S14), (S17), and (S18), the sensor behavior in terms of sensitivity and adsorption density can be simulated. In our simulation, Δq_a^+ and Δq_g^- are calculated from the Bader charge analysis in first-principles calculations for the phosphorene first, and then extrapolated to multilayer in the same manner as for the binding energy. The distance d between the adsorbed metal ions can be straightforwardly calculated as $d = 1/\sqrt{n_a}$. The parameter α is empirically taken as 1/2, namely, $d = 2D_e$, so that the scattering is mitigated by e^{-1} when Debye sphere touches each other. The effect of the parameter α lies in tuning the magnitude of sensitivity and the dynamic response range. Smaller value of parameter α would give rise to both a larger sensitivity and a wider dynamic response range.

Dynamic response simulation

Since the metal ions are well distributed in the solution before adsorption (i.e., no concentration gradient) and the size/volume of the metal ion solution is much larger than the surface area of the sensor; therefore, we could make the assumption that only the metal ions within certain region can diffuse and adsorb on the sensor surface. As illustrated in Figure S12, we define the region in the shape of semisphere with a radius of r_{max}. Thus, the metal ion adsorption density on the sensor surface with area A at time t can be obtained as

$$n_a(t) = \frac{1}{A}\int_0^t \rho \cdot 2\pi r^2 dr = \frac{2\pi}{3A}\rho r(t)^3 = \frac{2\pi}{3A}\rho v^3, v = \sqrt{2D \cdot s^{-1}} \quad \text{(S19)}$$

where v (D)is the velocity (diffusion coefficient) of the metal ions, s is time in the unit of second. From Equation (12) and (19), we can straightforwardly get r_{max}, namely,

$$r_{max} = \left(\frac{3n_a A}{2\pi\rho}\right)^{\frac{1}{3}} \tag{S20}$$

Similarly, the total response time t_{max} is

$$t_{max} = \frac{1}{v}\left(\frac{3n_a A}{2\pi\rho}\right)^{\frac{1}{3}}. \tag{S21}$$

Note that Equation (S21) is only valid for one-time measurements, since it only involves one specific value of metal ion concentration. Because the sensor test in our experiment was accumulative towards various concentrations, Equation (S21) has to be reformulated for each concentration as

$$t_{max}^{\ i} = \frac{1}{v}\left[\frac{3\left(n_a^i - \sum_0^{i-1} n_a^i\right)A}{2\pi\rho^i}\right]^{\frac{1}{3}}, \tag{S22}$$

in which i indicates the *i* th measurement with concentration ρ^i. In our simulations, the value of the diffusion coefficient D is taken as 8.47×10^{-10} m^2s^{-1} for Hg^{2+} ions.[11]

Supplementary References

(1) S. Cui, H. Pu, S. A. Wells, Z. Wen, S. Mao, J. Chang, M. C. Hersam, J. Chen, Ultrahigh sensitivity and layer-dependent sensing performance of phosphorene-based gas sensors, *Nat. Commun.* **2015**, 6, 8632

(2) J. A. Dean, *Lange's handbook of chemistry,* McGraw-Hill, 15 edn,**1999**.

(3) L. Pauling, *The chemical bond,* Cornell University Press, Ithaca,**1967**.

(4) T. L. Hill, *An introduction to statistical thermodynamics,* Dover Publications, Inc, New York,**1986**.

(5) H. H. Pu, S. H. Rhim, M. Gajdardziksa-Josifovska, C. J. Hirschmugl, M. Weinert, J. H. Chen, A statistical thermodynamics model for monolayer gas adsorption on graphene-based materials: Implications for gas sensing applications, *Rsc Advances* **2014**, 4, 47481-47487.

(6) Y. Marcus, A. Loewenschuss, Standard entropies of hydration of ions, *Annu. Rep. Prog. Chem. Sect. C: Phys. Chem.* **1984**, 81, 81-135.

(7) M. D. Tissandier, K. A. Cowen, W. Y. Feng, E. Gundlach, M. H. Cohen, A. D. Earhart, J. V. Coe, T. R. Tuttle, The proton's absolute aqueous enthalpy and gibbs free energy of solvation from cluster-ion solvation data, *J. Phys. Chem. A* **1998**, 102, 7787-7794.

(8) Y. Cai, G. Zhang, Y.-W. Zhang, Layer-dependent band alignment and work function of few-layer phosphorene, *Sci. Rep.* **2014**, 4, 6677

(9) L. Li, Y. Yu, G. J. Ye, Q. Ge, X. Ou, H. Wu, D. Feng, X. H. Chen, Y. Zhang, Black phosphorus field-effect transistors, *Nat. Nanotechnol.* **2014**, 9, 372-377.

(10) T. Vy, R. Soklaski, Y. Liang, L. Yang, Layer-controlled band gap and anisotropic excitons in few-layer black phosphorus, *Phys. Rev. B* **2014**, 89, 235319.

(11) J. Buffle, Z. Zhang, K. Startchev, Metal flux and dynamic speciation at (bio)interfaces. Part 1: Critical evaluation and compilation of physicochemical parameters for complexes with simple ligands and fulvic/humic substances, *Environ. Sci. Technol.* **2007**, 41, 7609-7620.